



Seventh Framework Programme

Theme 6

Environment



Project: 603864 – HELIX

Full project title:

High-End cLimate Impacts and eXtremes

Deliverable: 4.1

D4.1. Documentation of impact emulators and demonstration of their applicability
in highly efficient impact projections for selected key regions

Katja Frieler

Version 1.0

Original Due date of deliverable: 10/31/2016

Actual date of submission: 10/31/2016

Contents

1. Methods	4
1.1 Basic non-parametric approach – changes in crop yields in terms of global mean temperature change	4
1.2 Linear scaling - Projections of flood volume and mean precipitation for individual river basins ...	6
1.3 Process-based approach – Changes in global average vegetation carbon	6
1.4 Accounting for delayed responses – The “constrained extrapolation approach”	7
2. Results	8
2.1 Performance basic non-parametric approach for changes on crop yields	8
2.2 Projections of flood volume for individual river basins.....	10
2.3 Performance of the reduced form model for global vegetation carbon.....	13
2.4 Results for the emulator of sea level changes	16
3. Conclusion	19
4. Acknowledgements	20
5. References.....	20

Executive summary

PIK developed reduced form impact models for

- 1) Changes in crop yields for maize, wheat, rice and soy (spatially explicit patterns)
- 2) Changes in flood volume and mean and extreme precipitation (average across most important river basins)
- 3) Changes in vegetation carbon (global average)
- 4) Sea level rise accounting for thermal expansions, contributions from mountain glaciers and the Greenland and Antarctic ice sheet (spatially explicit patterns).

The approaches range from a basic “binning approach” (see “basic non-parametric approach” below) where the simulated impact is averaged across certain global mean temperature intervals and linearly interpolated in between without prescribing the functional form of the relationship between global warming and the considered impact across the entire warming range (item 1), via a linear scaling (item 2), and a more process-based description based on separate representations of source and sink terms of global vegetation carbon (item 3) to a method allowing for the representation of time lags in the response to global mean temperature change as particularly relevant for sea level rise (item 4).

Projections for flood volume, global vegetation carbon, and crop yields account for the inter-impact-model spread of simulations generated within the ISIMIP fast track while sea level projections build on a careful evaluation of different observational data sets and long term equilibrium projections from different process-based or empirical models to represent the uncertainties of the projections.

While the approach for vegetation carbon allows for projecting global average vegetation carbon the other approaches are spatially explicit allowing for projecting changes in flood volume for individual river basins and crop yields or sea level rise on a global grid. For sea level rise we developed individual emulators for each contribution (thermal expansion, loss of Greenland’s ice sheet, loss of Antarctic ice sheet and loss of mountain glaciers). In this way the approach does not only account for individual response times of the different systems and temporally varying contributions to overall sea level rise but also opens the possibility to represent gravitational effects, i.e. individual spatial finger prints e.g. associated with the loss of ice masses from Greenland and Antarctica. These effects generally lead to higher hazards in tropical regions than in high or low latitudes (Perette et al., 2013).

On the one hand the emulators represent efficient tools to estimate impacts associated with emission pathways not originally translated into spatially explicit patterns of climate change by Global Circulation Models and associated regional impacts by complex process-based impact models. Instead emission scenarios could be translated into global mean temperature (and CO₂ concentration) pathways by simple climate models such as MAGICC (Meinshausen, Raper, and Wigley 2011) which are then used as input for the emulators “scaling” the impacts from available complex model simulations to the new scenario. On the other hand, the synthesis of impacts associated with the development of simplified representations of complex model simulations particularly allows for a better understanding of the underlying processes and

sources of inter-impact model spread. Thus, we particularly focus on the separation of gain and loss processes and their dependence on climate and CO₂ changes when describing changes in vegetation carbon and differences between projected changes in mean precipitation, extreme precipitation and flood volume to get a better quantitative understanding of the underlying dynamics of changes in flood risks.

1. Methods

In the framework of the Inter-Sectoral Impact Model Intercomparison Project (Warszawski et al. 2014), a set of impacts models from different sectors were driven by climate projections from five different Global Circulation Models (GCMs: HadGEM2-ES, IPSL-CM5A-LR, MIROC-ESM-CHEM, GFDL-ESM2M, and NorESM1-M) and for four Representative Concentration Pathways (RCPs). The daily climate input data were bias-corrected toward an observation-based dataset (WATCH, Weeden et al. 2011) using a trend-preserving method (Hempel et al. 2013). The impact models were run without direct coupling to GCMs, so potential feedbacks were not represented.

We use daily runoff projections from eight global hydrological models, one global land-surface model, and one dynamic global vegetation model (summarized as global hydrological models, or GHMs); crop yield projections of six Global Gridded Crop Models (GGCMs) for wheat, maize, rice and soy; and simulations of global vegetation carbon from six Global Vegetation Models (GVMs). In the latter case the analysis was restricted to HadGEM2-ES as for this model impact modellers also provided “fixed CO₂” runs where climate was varied but CO₂ was held fixed at present day levels.

The sea level projection where based on CMIP5 simulations for thermal expansion and different process-based ice sheet models

1.1 Basic non-parametric approach – changes in crop yields in terms of global mean temperature change

The emission of greenhouse gases is expected to influence crop yields via several channels. On the one hand the associated climate changes will modify the length of the growing season (Eyshi Rezaei et al. 2014), water availability, and heat stress (Lobell, Sibley, and Ivan Ortiz-Monasterio 2012; Müller and Robertson 2014; Schlenker and Roberts 2009); and on the other hand higher concentrations of atmospheric CO₂ are expected to increase the water use efficiency in C3 (e.g. wheat, rice, soy) and C4 (maize) crops, and enhance the rate of photosynthesis in C3 crops (Darwin and Kennedy 2000). Global Gridded Crop Models (GGCMs) are particularly designed to account for these effects. They provide a complex process-based implementation of our current understanding of the underlying mechanisms and are the primary tools for (long-term) crop yield projections (Rosenzweig et al. 2014).

We tested to what degree the ISIMIP crop yield projections can be directly described in terms of global mean temperature (and CO₂) changes, i.e. to what degree the mean changes in crop yields derived for specific global mean temperature or CO₂ levels are independent of the underlying temporal evolution of emissions. To this end we compared the spread in yield outcomes at given levels of global warming (separated by 0.5°C steps with 0.5°C width) that is induced by the choice of emission scenario (four RCPs)

to the spread induced by the choice of the crop model (six GGCMs) and the GCM (5GCMs), respectively. The quantification is based on a one-way analysis of variance (ANOVA fixed effects model). A low scenario-induced spread means that GCM- and crop model-specific yield projections can be approximated by a simplified relationship with global mean temperature change without accounting for the underlying emission scenario, i.e. RCP-based projections could be efficiently translated to other global mean temperature pathways by referring to the associated binned yields. The test is done at each grid cell and separately for simulations of purely rain-fed yields and fully irrigated yields. Separate simulations are available for each of the four major crops: wheat, maize, rice and soy, on a global 0.5 x 0.5 degree grid. The considered crop is assumed to grow everywhere on the global land area, only restricted by soil characteristics but independent of present or future land use patterns (“pure crop” simulations). This design provides full flexibility with regard to the application of future land use and irrigation patterns in post-processing. While the default crop yield simulations (Y_{CO_2}) account for the CO_2 fertilization effect, the setting also includes a sensitivity experiment where the impact models were forced by climate change projections from HadGEM2-ES, RCP8.5 but CO_2 concentrations were kept fixed at a “present day” reference level ($Y_{fixedCO_2}$). In a very basic set-up patterns of changes in crop yields for a given level of global warming are derived from an interpolation between the patterns averaged across the neighboring global mean warming bins where the average pattern for the discrete bins are derived from the RCP8.5 projections of the individual climate and crop model simulations accounting for the CO_2 fertilization effect (Method 1). As varying levels of CO_2 at fixed global warming levels may explain part of the scenario dependence of the global mean temperature response, we additionally evaluate two approaches to estimate the direct CO_2 effect on crop yields within the different global mean temperature bins:

a) Method 2: By linear regression of absolute yield changes (ΔY_{CO_2}) with respect to the historical reference period on CO_2 concentration within the individual global mean warming bins, i.e. by fitting the following model

$$\Delta Y_{CO_2, i} = a_0 + a_1 * (pCO_{2,i} - 370 \text{ ppm}) + \epsilon_i, \quad (1)$$

where i indicates the individual year, and $\epsilon_i \sim N(0, \sigma^2)$ represents the residual error. The statistical model allows for the estimation of the purely climate induced changes a_0 at a fixed year 2000 concentration of CO_2 of 370 ppm.

b) Method 3: By linear regression of the within-bin differences between the default crop simulations (Y_{CO_2}) and the fixed CO_2 run ($Y_{fixedCO_2}$) on the underlying CO_2 concentration:

$$(Y_{CO_2, i} - Y_{fixedCO_2, i}) = a_0 + a_1 * (CO_{2,i} - 370 \text{ ppm}) + \epsilon_i, \quad (2)$$

where i indicates the individual year and $\epsilon_i \sim N(0, \sigma^2)$ represents the residual error.

To evaluate and compare the performance of the two approaches we consider large scale regional average yields based on fixed present day (1998-2002) land use and irrigation patterns from MIRCA2000 (Portmann, Siebert, and Döll 2010) and assess the reproducibility of the original RCP2.6, RCP4.5, and RCP6.0 projections based on the emulated yield patterns (see section 2.1).

1.2 Linear scaling - Projections of flood volume and mean precipitation for individual river basins

All combinations of daily runoff data (50 combinations each for historical and the four RCP simulations) are translated into daily flood volume by CaMa-Flood (version 3.44, Dai 2011) at a 0.25 degree global grid. For 12 most populous river basins worldwide annual maximum flood volume is derived from basin total daily flood volume. To describe changes in maximum flood volume in terms of global mean temperature change we applied a linear mixed model assuming a linear relationship between flood volume and global mean warming. The statistical model allows for scenario specific random deviations (random effects) from a common scaling coefficient (fixed effect). For each river basin we estimate fixed effects and standard deviations of the random effects for each climate- and impact model combination. Because no change in annual maximum flood volume is expected at 0 degree of global warming, the intercept is assumed to be 0. The same method was applied to annual mean precipitation and annual maximum of daily mean precipitation across the river basins.

The estimated standard deviation of the scenario specific random effects is considered as an indicator of the validity of the simple scaling approach: If the coefficients only show a minor scenario dependence the common fixed effect could be used to scale changes in flood volume with global mean temperature to translate the changes derived for the four RCP scenario to other global mean temperature pathways.

1.3 Process-based approach – Changes in global average vegetation carbon

Global vegetation carbon can be described in terms of the following balance equation:

$$\frac{dC_{veg}}{dt} = NPP - \frac{C_{veg}}{\tau} \quad (3)$$

Accordingly, in a first step individual emulators were developed for the net primary productivity (NPP) and the residence time of carbon in vegetation (τ). In a second step, these emulators were combined to allow for modelling C_{veg} .

After aggregating the NPP and C_{veg} GVM output at the global annual scales, time-series of τ were extracted from the discrete version of Eq. (3). A similar procedure was applied to simulations performed with CO_2 concentrations kept constant at present day values to disentangle the signals of climate and CO_2 forcing. For each variable, the simulations with fixed CO_2 (“fixed CO_2 ”) were subtracted from the default ones generating new time-series isolating the effects induced by changes in CO_2 .

The functional form of the NPP emulator consists of a linear relation to global mean temperature $T(t)$ at time t and a Michaelis-Menten function for CO_2

$$NPP = (a_1 + a_2 T(t)) \frac{a_3 CO_2}{a_4 + CO_2} \quad (4)$$

The regression coefficients a_1 and a_2 were obtained by fitting the linear relation to the simulations with fixed CO_2 . Consecutively, coefficients a_3 and a_4 were extracted by applying a regression to the default NPP simulations, taking simultaneously $T(t)$ and CO_2 as predictors. For the residence time, a linear relationship between τ and $T(t)$ was assumed.

We test the performance of the emulator by 1) using RCP8.5 as training data and predicting the response for the other scenarios and 2) by consecutively using a combination of three RCPs as training data set and trying to predict the other. The second approach was chosen to test whether responses to lower levels of warming (RCP2.6 + RCP4.5 + RCP6.0) can be extrapolated to higher levels (RCP8.5) while the first approach particularly allows for testing whether the response to lower levels of warming can be predicted based on the response to high levels of warming.

1.4 Accounting for delayed responses – The “constrained extrapolation approach”

The ocean as well as the ice sheets show a delayed response to global warming. As a consequence, sea level is expected to rise for centuries to come even under strict reductions in greenhouse gas emissions (Gillett et al. 2011; IPCC 2013; Meehl, Arblaster, and Tebaldi 2005; Solomon et al. 2009; Wigley 2005). While the long-term equilibrium response of sea level rise to global temperature changes can be constrained by paleoclimatic data and is more easily computed with currently available process-based large-scale models, the rate of change is still difficult to project. On the other hand there is an increasing number of observations of last century’s contributions to sea level rise from the individual components. We developed an approach that combines the estimates of the equilibrium sea level rise at certain levels of global warming with historical observations. To this end we assume that the change of sea level S due to each considered component can be described the following differential equation (pursuit curve)

$$\frac{dS}{dt} = \frac{S_{eq}(T(t),\alpha) - S(t)}{\tau} \quad (5)$$

where S_{eq} is the equilibrium contribution as a function of the global mean temperature $T(t)$ and a commitment factor α . The commitment factor is derived from estimates of the long term response for the major contributing processes (thermal expansion, loss of mountain glaciers, Solid Ice Discharge (SID) from Antarctica and changes in the Surface Mass Balance (SMB) of Greenland). The ordinary differential equation describes a physical system in which S approaches its equilibrium value with speed linearly dependent on the deviation from the equilibrium and the inverse of τ . Given S_{eq} the “delay parameter” τ is estimated from a range of historical observations (Mengel et al. 2016). Slightly different approaches are applied the minor contributions from Greenland SID and Antarctic SMB.

The spatial pattern of dynamic and density-related sea level changes can be diagnosed directly from GCMs. In addition, regional variations of sea-level rise from glaciers and the large ice sheets not considered in GCM simulations can be derived by scaling from their respective gravitational patterns. These patterns are assumed to be time and scenario independent. Total climate-driven sea-level rise at a certain location is the sum of the patterns for dynamic sea-level changes, glaciers and ice caps and the Greenland and the Antarctic ice sheet.

The method allows for fast and transparent sea level rise projections for scenarios not covered by process-based model simulations such as the HELIX scenarios or the ISIMIP2b scenarios designed to allow for an assessment of climate change impacts for the planned IPCC Special Report on the impacts of 1.5°C of global warming. The method is applied to provide this critical input for the coastal impact models (Frieler et al.

2016). To this end the approach has been extended to ensure a smooth transition from historical patterns of sea level rise and future projections.

2. Results

2.1 Performance basic non-parametric approach for changes on crop yields

The analysis shows that the choice of the emission scenario only explains a minor component of the overall variation of crop yields within a given global mean temperature bin (see Figure 1 for rainfed yields at a level of 2.5°C of global warming above 1980-2010 levels).

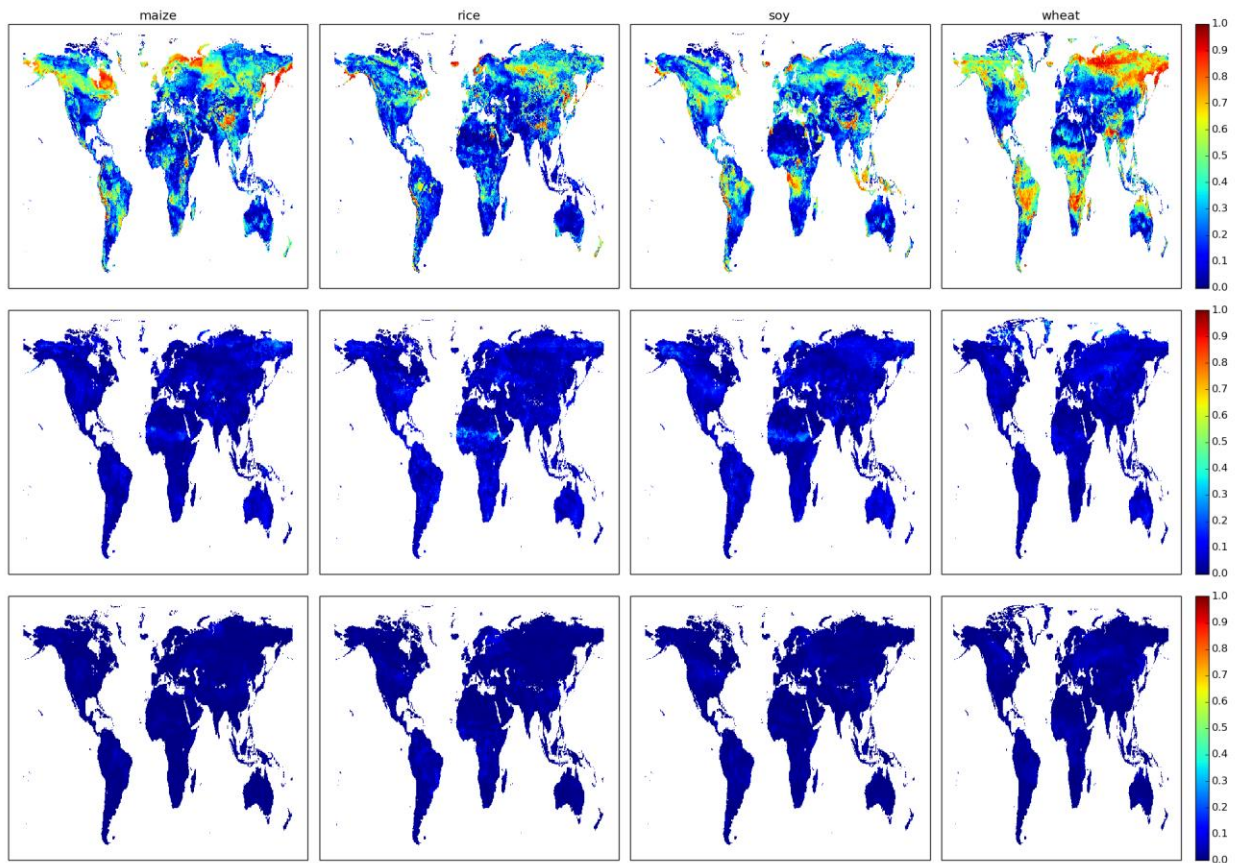


Figure 1: Variance attributable to the GGCM (top row), GCM (middle row), and scenario (bottom row) for each crop. Plot shown for “rain-fed” runs at $T(t)=2.5^{\circ}\text{C}$ warming.

Applying the three methods described in Section 1.1 does not reveal significant advantages of one individual method. In contrast, the very basic interpolation approach seems to be sufficient for the range of RCP scenarios considered (when training the emulator on the high emission scenario RCP8.5 and predicting the other three RCPs) (see Figure 2).

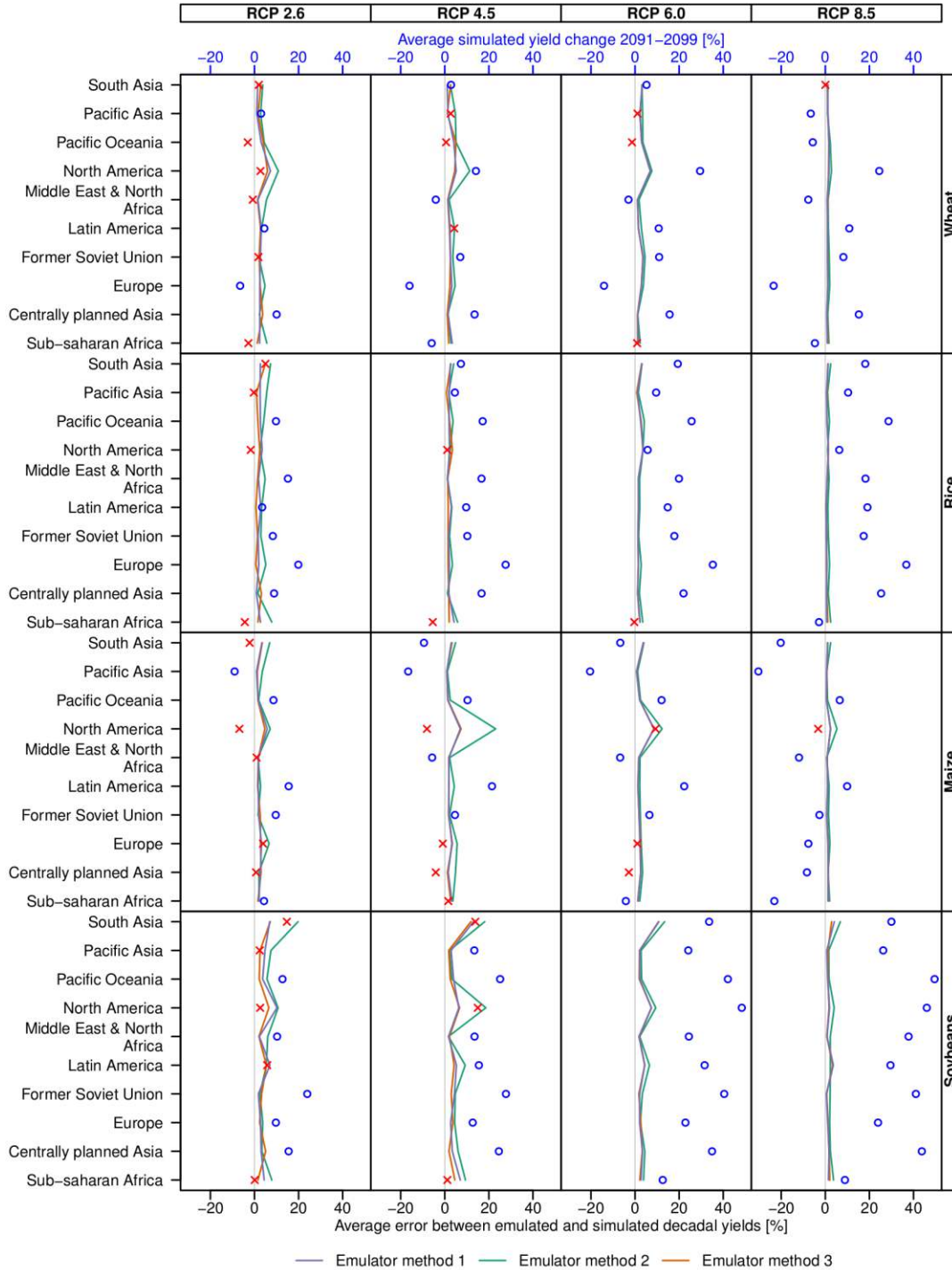


Figure 2: Root mean square deviation of the LPJmL simulations forced by HadGEM2-ES climate projections and the associated emulations for RCP2.6, RCP4.5, and RCP6.0. The emulators (Method 1, 2, and 3 described in section 1.1) are trained on RCP8.5. For comparison, blue points illustrate the average simulated yield change for 2091 – 2099 if the absolute value of the change is larger than the root men square deviation between simulated and emulated yields while red crosses were used otherwise.

The very basic interpolation approach (Method 1) allows for a relatively close emulation of the regional average changes in crop yields as provided by the process-based crop models for RCP2.6, RCP4.5, and RCP6.0 (see

Figure 3 for HadGEM2-ES and the LPJmL crop model). The relatively large inter-annual variability of simulated crop yields is not expected to be captured by the emulator.

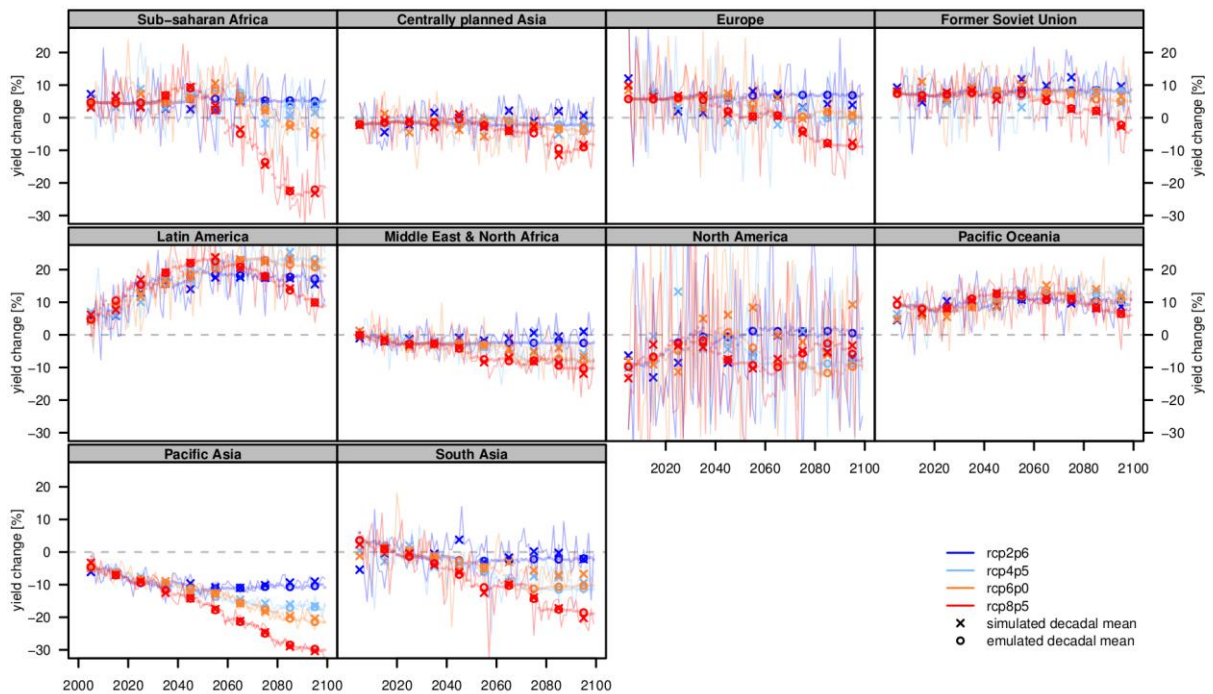


Figure 3: Comparison of simulated and emulated time series of regionally averaged crop yield changes for LPJmL forced by HadGEM2-ES climate projections. Regional averages are calculated based on fixed present day land use and irrigation patterns. Results are shown for Maize and emulator method 1.

2.2 Projections of flood volume for individual river basins

In general the scenario-dependence of the scaling coefficients turned out to be low (see grey shaded areas around regression lines described by the fixed effects) for simulated flood volume (Figure 4) as well as for basin average precipitation changes (Figure 5), and extreme precipitation (Figure 6). Thus, the simplified approach allows for a first order approximation of the changes in terms of global mean temperature

change. The estimated standard deviations of the scenario specific random effects particularly allow for representing the spread of the associated projections that is induced by the remaining scenario dependence of the scaling coefficients. As can be seen from Table 1, the scenario specific random effects are generally small in most basins both for flood volume and precipitation.

Scaling coefficients strongly change from basin to basin. Flooding is more intense with heavier basin-wide rainfall and under a wetter prior soil condition. Therefore, the scaling coefficients of annual maximum flood volume (Figure 4) are related to both scaling coefficients of mean (Figure 5) and maximum precipitation (Figure 6): the former is associated with variation in soil water condition, and the latter is related to potential water “available” for flooding. Generally, the scaling coefficient for flood volume would be closer to that of mean precipitation if the prior soil condition allows holding more water from flooding. This is the case in basins with a dryer climate such as the Yellow River and Nile River basins (Table 1). In basins with a wetter climate such as Amazonas and Mississippi, the scaling coefficient for flood volume is closer to that of maximum precipitation. The scaling coefficients for flood volume are found to be notably higher than those of maximum precipitation in a number of basins (Yangtze, Ganges, Indus and Pearl), all of which are under heavy influence from monsoon climate. Under such weather system it is typical that consecutive days of very heavy rainfall can occur in one single event, causing an accumulation of flood water in river basins. As a result, the scaling coefficient for annual maximum flood volume can be larger compared to that of extreme precipitation for these basins.

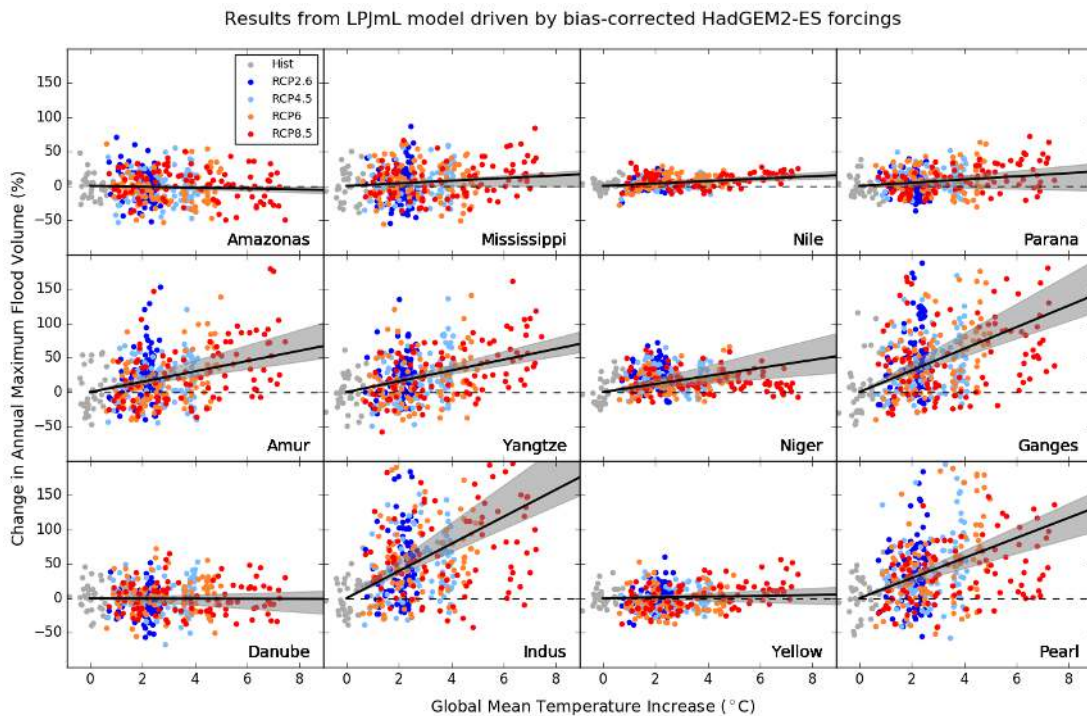


Figure 4: Change in maximum annual flood volume in term of global mean temperature changes. Red dots: RCP8.5; grey dots: historical simulations; dark blue dots: RCP2.6, light blue dots: RCP4.5, and orange dots:

RCP6.0. Black line: slope derived from the estimated fixed effect; shade: full range of slopes derived from the four RCPs.

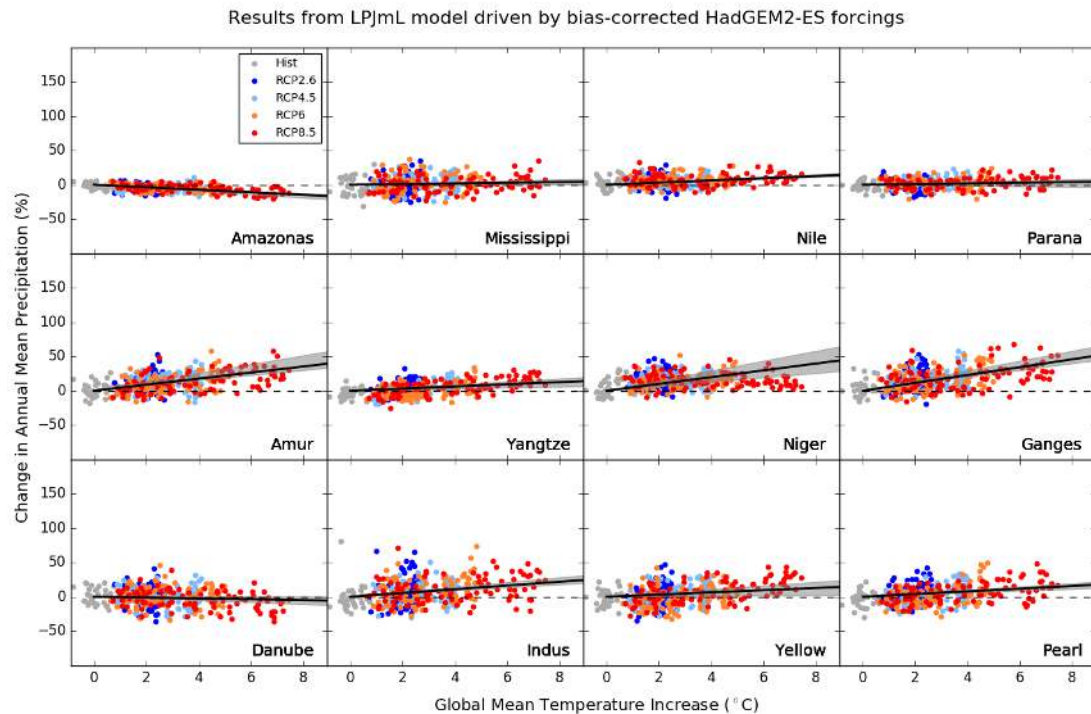


Figure 5: Change in annual mean precipitation in term of global mean temperature changes. Red dots: RCP8.5; grey dots: historical simulations; dark blue dots: RCP2.6, light blue dots: RCP4.5, and orange dots: RCP6.0. Black line: slope derived from the estimated fixed effect; shade: full range of slopes derived from the four RCPs.

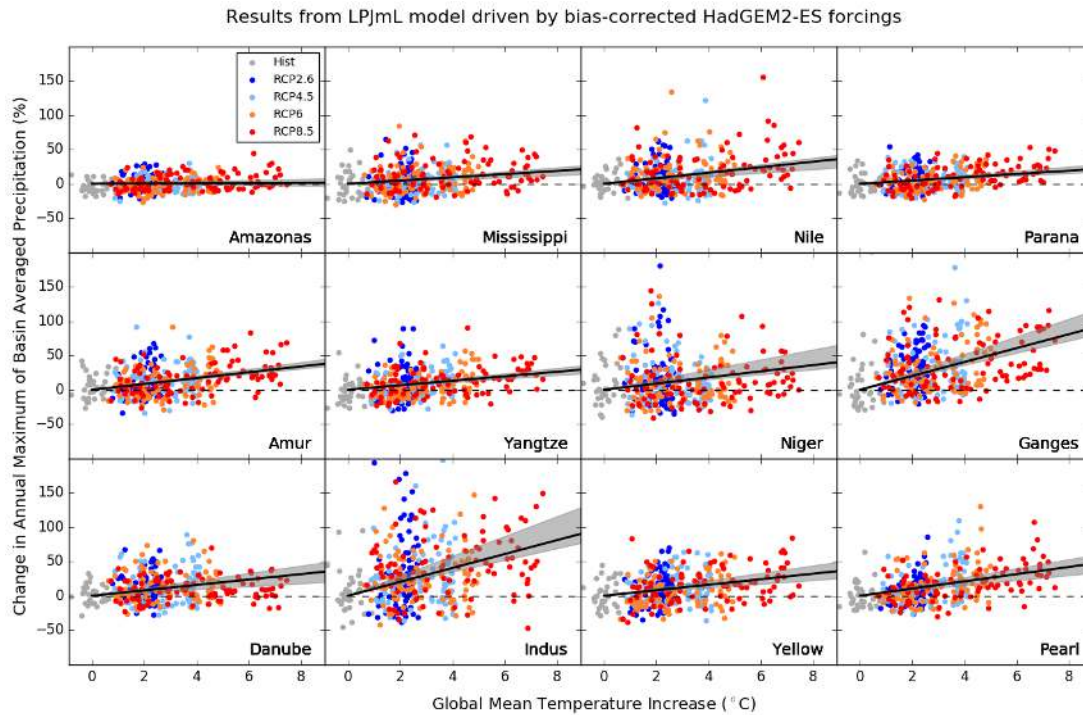


Figure 6: Change in annual maximum of basin-averaged daily precipitation in term of global mean temperature changes. Red dots: RCP8.5; grey dots: historical simulations; dark blue dots: RCP2.6, light blue dots: RCP4.5, and orange dots: RCP6.0. Black line: slope derived from the estimated fixed effect; shade: full range of slopes derived from the four RCPs.

Table 1: Scaling coefficients (fixed effects, their standard errors and the standard deviation of the random effects) for changes in annual maximum flood volume, changes in mean and maximum annual precipitation per degree of global mean temperature change. All estimates are derived from the combination of HadGEM2-ES and the GHM LPJmL. Other combinations are also computed.

	Fixed effect (flood volume)	standard deviation of scenario specific random effects (flood volume)	Fixed effects (mean precipitation)	standard deviation of scenario specific random effects (mean precipitation)	Fixed effects (maximum precipitation)	standard deviation of scenario specific random effects (maximum precipitation)
Amazonas	-0.6%±0.5%	0.0%	-1.8%±0.2%	0.3%	0.2%±0.3%	0.5%
Mississippi	1.9%±0.8%	0.2%	0.5%±0.2%	0.0%	2.3%±0.4%	0.3%
Nile	1.7%±0.3%	0.5%	1.6%±0.1%	0.0%	4.0%±0.5%	0.7%
Parana	2.3%±1.0%	1.8%	0.5%±0.3%	0.5%	2.4%±0.3%	0.4%
Amur	7.5%±1.2%	1.9%	4.4%±0.6%	1.1%	4.2%±0.3%	0.0%

Yangtze	7.9%±0.6%	0.2%	1.6%±0.3%	0.5%	3.3%±0.3%	0.0%
Niger	5.8%±1.4%	2.6%	4.9%±0.8%	1.6%	4.5%±1.1%	0.0%
Ganges	15.7%±1.9%	3.3%	5.7%±0.5%	0.7%	10.1%±0.8%	0.9%
Danube	-0.1%±0.7%	1.1%	-0.6%±0.4%	0.6%	3.9%±0.7%	1.2%
Indus	19.8%±2.2%	3.6%	2.7%±0.5%	0.0%	10.1%±0.7%	0.7%
Yellow	0.6%±0.7%	1.3%	1.6%±0.6%	1.0%	4.0%±0.5%	0.5%
Pearl	14.6%±1.6%	2.7%	2.0%±0.2%	0.0%	5.2%±0.5%	0.6%

2.3 Performance of the reduced form model for global vegetation carbon

NPP emulation: The global NPP responses in the ISIMIP ensemble to climate change are determined by the counteracting effects of a positive influence of CO₂ fertilization, on one hand, and the negative influence induced by climate in isolation, on the other. This competition results in a linear increase in NPP along with global mean temperature, which is observed in all the GVMs except Hybrid.

Using global mean temperature and CO₂ as predictors, the mean differences between emulated and simulated NPP changes are mostly below 5%, with the exception of Hybrid (8%). When only considering climate change in isolation from CO₂-effects, the performance is similar. Moreover, the emulation matches the GVM pattern in the historical period which has not been included in model training.

Carbon residence time: The responses of τ to global warming are less consistent across GVMs than the NPP response. The sensitivity to global warming is positive in Hybrid and ORCHIDEE and negative in JULES, JEDI, VISIT and LPJmL (Friend et al. 2014). We find that differences in the dynamics of τ across models are mostly attributed to the influence of CO₂.

When isolating the effect of climate, the responses of τ to changes in CO₂ exhibit a hysteresis effect, that becomes visible along the CO₂ stabilization phases in RCP2.6 and RCP4.5. For this reason, a faithful representation of the response of τ to CO₂ requires accounting for the contribution of lag terms in CO₂. In spite of this, for the purpose of emulating the response of τ in the high-end RCP8.5 scenario, the dependence of τ on CO₂ trajectories can be omitted in a first approximation. Indeed, assuming a linear relation with global mean temperature allows one to reproduce the GVM responses with an overall mean error below 6% across the 4 RCPs. The shortcoming of such a simplification is clearly a limited accuracy in the emulation of τ along CO₂ stabilization phases, as well as an inadequate extrapolation of the historical period – in contrast to the emulation of NPP.

Vegetation Carbon: A positive trend in C_{veg} is observed for all the GVMs except for LPJmL and Hybrid, where the increase in C_{veg} saturates, followed by a decrease towards higher warming levels (Figure Figure 7). The ratio of climate to CO₂ induced effects on C_{veg} varies largely between models, from 40-75% in JULES (for RCP8.5, at end of century), SDGVM, ORCHIDEE and JeDi up to 106% and even 285% in LPJmL and Hybrid, respectively. These differences can be mostly attributed to the different behaviors of τ .

The emulated responses of C_{veg} to climate change obtained via numerical integration of Eq. (3), in combination with the NPP and τ emulators, have associated mean errors in the range 1.07 % (VISIT) – 3.31

% (SDGVM) and successfully emulate the response of the GVMs to high-level warming (Figure 7) in the default case, hence including increasing CO₂ and climate change as drivers. The emulator does not reproduce C_{veg} responses to a changing climate and fixed CO₂ for LPJmL and JULES under all warming levels and basically all GVMs when considering high-level warming. However, even for the “default” case, the emulation fails at resolving the stabilization phase in RCP2.6 and RCP4.5, occurring at around 1.5°C and 2.5°C of global warming, respectively. We find that a linear relationship of τ with CO₂, considered as additional predictor, does not improve the emulation of C_{veg} along stabilization phases in CO₂ trajectories –thus pointing to the need of explicitly accounting for memory effects in the response to CO₂.

To better account for the stabilization phases, we introduced a new formulation:

$$\frac{dC_{veg}}{dt} = \eta NPP \quad (6)$$

where $\eta = \frac{\tau - \tau_B}{\tau}$, and τ_B denotes the balance condition $\tau_B = C_{veg}/NPP$ in Eq. (3). η is sensitive to changes in the predictors. In particular, a reduced scenario dependence is observed in the scaling of η with the interannual variations of CO₂. We took advantage of this fact as a most simple mean to introduce memory into the dynamics of C_{veg}. After applying cross-validation on the quadratic function:

$$\eta = c_1 \frac{dCO_2}{dt} \left(1 - c_2 \frac{dCO_2}{dt}\right) \quad (7)$$

This new formulation improved the emulation of C_{veg} for the RCPs depicting CO₂ stabilization phases for the GVMs VISIT, JeDi, JULES and SDGVM. In combination with the NPP emulator, this formulation allowed to mimic the stabilization responses of C_{veg} to CO₂ in the aforementioned GVMs with an error below 5%. However, this method fails at extrapolating the high-end response in RCP8.5.

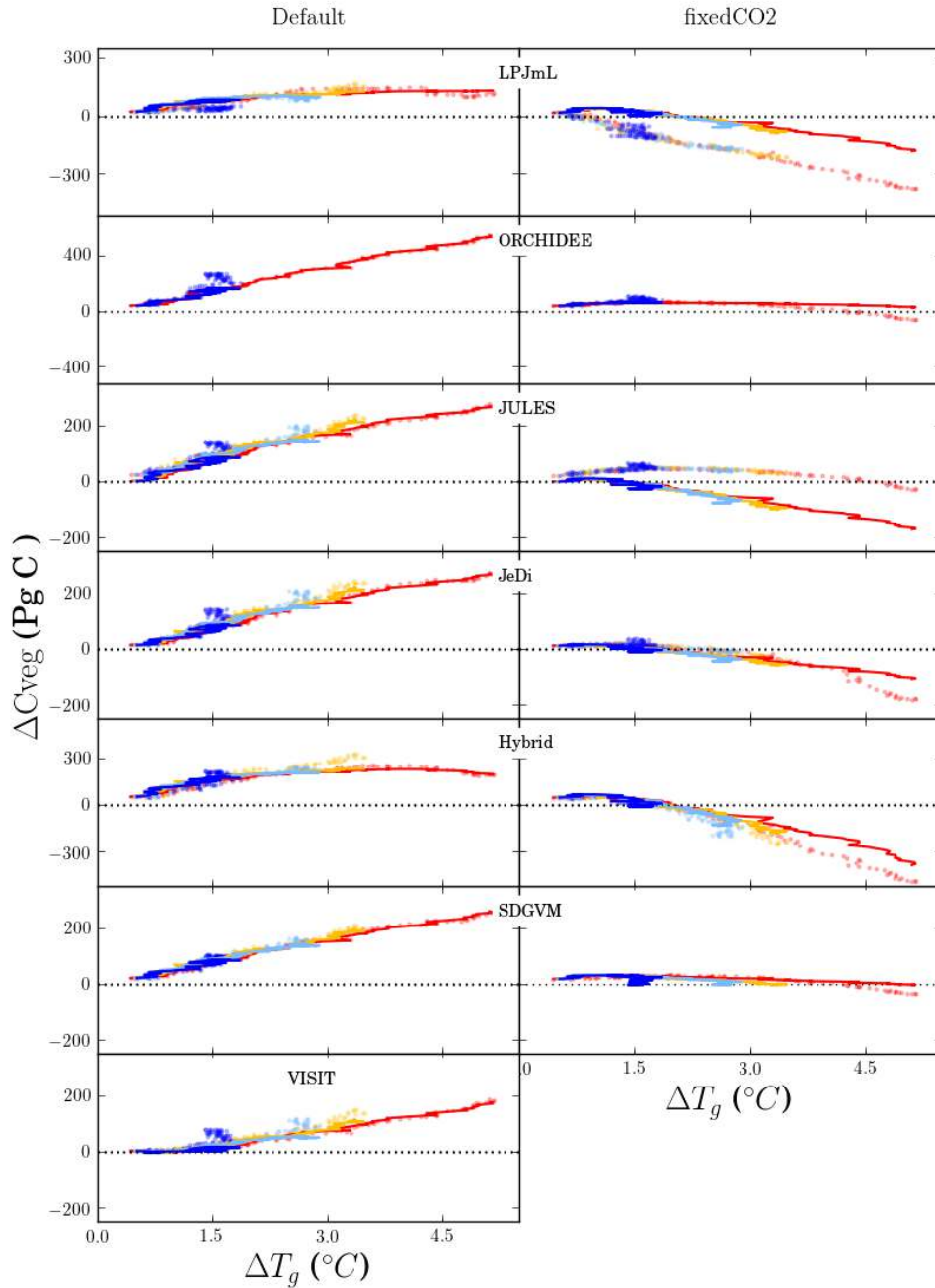


Figure 7: Responses of vegetation carbon to changes in global mean temperature $T(t)$ and atmospheric CO_2 concentrations. Solid lines show the emulation resulting from fitting the emulator to the RCP8.5 response. The emulations start with initial conditions being the first value of the RCP runs. Left column: the default simulations with increasing CO_2 . Right column: simulations with CO_2 concentrations held constant. Dark blue dots: RCP2.6, light blue dots: RCP4.5, orange dots: RCP6.0, and red dots: RCP8.5. Changes in all of the variables are considered with respect to the mean over the reference period 1980-2004. Note that for SDGVM and ORCHIDEE only a subset of fixed CO_2 runs are available (only RCP2.6 for SDGVM and only RCP8.5 and RCP2.6 for ORCHIDEE). Note that the emulation for the “fixed CO_2 ”

simulations has been carried out using the NPP coefficients obtained from fitting the NPP response of “fixedCO₂” simulations and τ fitted on the “default” simulations. This is to illustrate (indirectly via emulation of C_{veg}) the influence of CO₂ on τ .

We conclude that emulators for NPP, carbon residence time and vegetation carbon can basically represent the patterns simulated by complex global vegetation models. However, for the emulation of vegetation carbon, there is a trade-off between emulators being either able to match the stabilization phase of RCP2.6 and RCP6.0 or being able to match responses to high-level warming. However, emulation of responses in stabilization and high RCPs can be accomplished if the emulator is simultaneously trained on RCP8.5 and RCP2.6, which then would allow to emulate the range of trajectories between these two RCP scenarios.

2.4 Results for the emulator of sea level changes

Past contributions of sea level rise can generally be well reproduced by the presented model (Figure 8) Thermal expansion lies within the range of process-based CMIP5 models. Glaciers are underestimated for the very early part of the calibration period for the Leclerc et al. 2011 dataset (Leclercq, Oerlemans, and Cogley 2011), indicating that the early glacier contribution, attributed to the so-called early Arctic warming, cannot be well related to global mean temperature change. Our approach can reproduce the Greenland's past contribution based on three diverse Greenland datasets. The high observational uncertainty translates into broad uncertainty ranges for the projected contribution of Greenland. Calibrated Antarctic solid ice discharge well reproduces the three datasets. We find particularly large “delay parameters” for Antarctica, as expected. This is due to the slow response of Antarctic ice flow to warming.

Our approach reproduces the past total climate-driven sea level rise reasonably well, although it is not used for the calibration (Figure 9). This provides confidence that the method captures the major processes of sea level rise. Early 20th century is underestimated, indicating that not all sea level rise was driven by anthropogenic climate change during that period rather than falsifying the presented approach.

All future projected sea level contributions are scenario dependent by design (Figure 10). We find future thermal expansion similar to the IPCC (IPCC 2014; IPCC 2013). Mountain glaciers show weak scenario sensitivity due to the limited world glacier volumes. While Greenland SID and Antarctic SMB stay relatively small, Greenland SMB shows a large contribution and high scenario spread because of the high sensitivity for strong warming. Climate-driven Antarctic ice loss is a minor contributor to future sea level rise due to its slow response time.

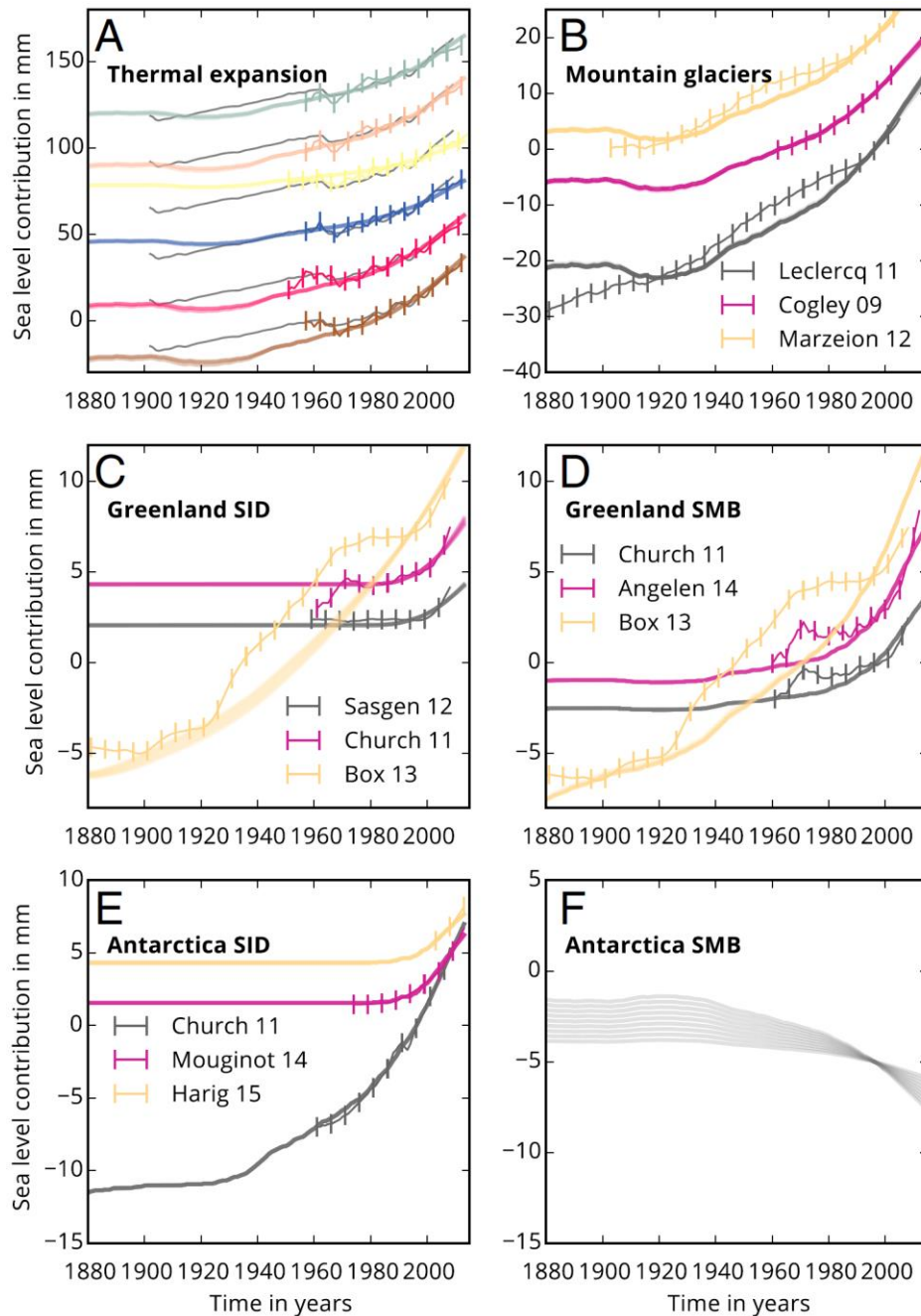


Figure 8: Observed and calibrated sea-level contributions. Observed (lines with bars) and calibrated sea-level contribution (lines) during the calibration period for each sea-level component. (A) subset of combinations of upper, middle and deep ocean thermal expansion. Grey lines show CMIP5 model mean. (B) Anthropogenic mountain glacier loss (C) Greenland solid ice discharge (D) Greenland surface mass balance (E) Antarctic solid ice discharge. The Antarctic SMB contribution (F) is not calibrated and provided for comparison. All timeseries relative to the 1986-2005 mean. An offset is applied between datasets for better visibility.

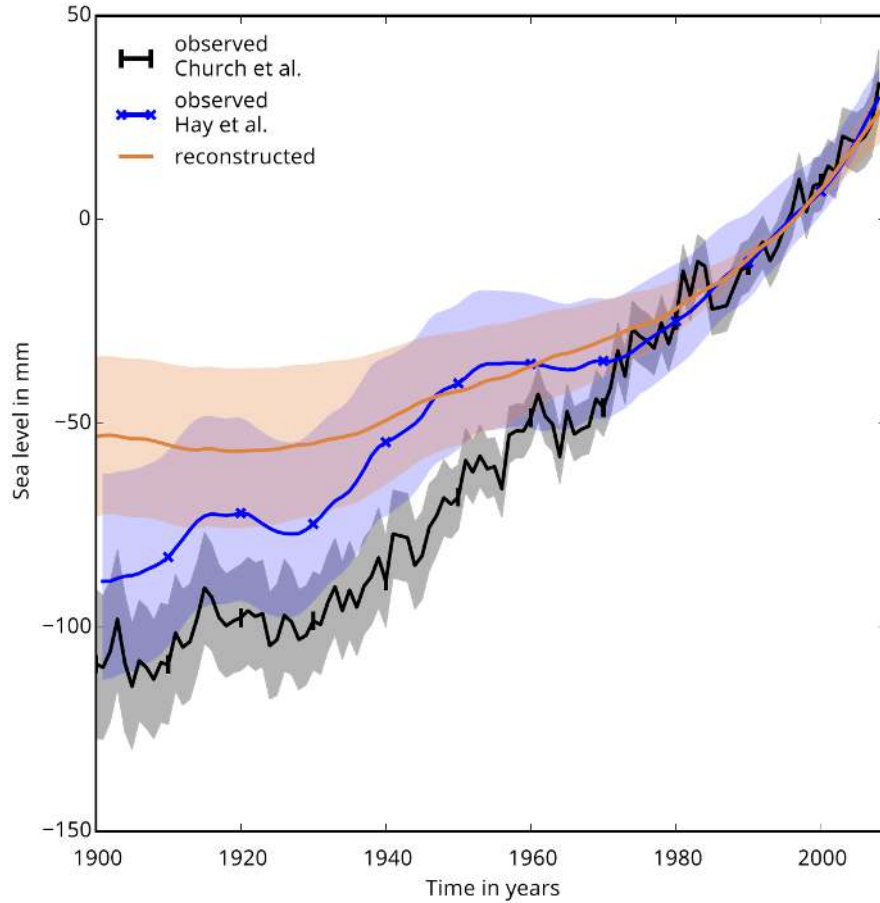


Figure 9: Reconstructed and observed total anthropogenic sea-level rise 1900-today. Reconstructed sea-level rise since 1900 as the sum of the probabilistically-combined single contributions (median as brown line and 90% uncertainty range as shading) and observed sea-level (blue: (Hay et al. 2015), black: (Church and White 2011); respective uncertainty ranges as shading). Only the anthropogenic part of the observed sea-level is shown, produced by subtraction of the non-anthropogenic glacier contribution. All timeseries relative to the 1986-2005 mean.

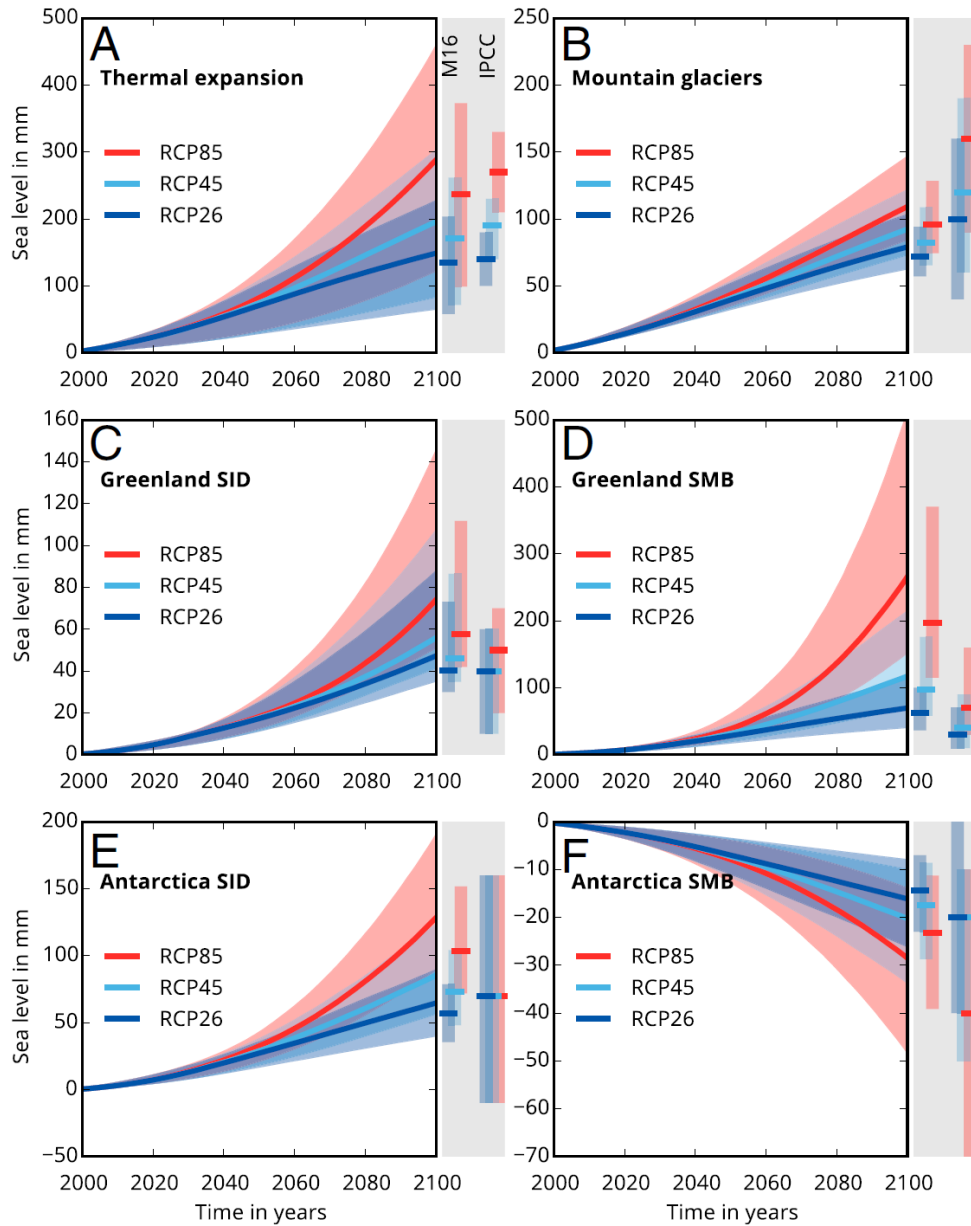


Figure 10: Projected contributions to 21st century sea-level rise. Median (thick line) and 5th to 95th percentile uncertainty range (shading) of projected single contributions for the three RCP scenarios; based on 10000 individual sea-level curves. Bars at the right show 5th to 95th percentile range of this study (M16) and the IPCC likely ranges intersected by the median for the 2081-2100 time mean. All relative to the 1986-2005 mean.

3. Conclusion

The impact emulators will allow for highly efficient impact projections based on arbitrary temperature and CO₂ concentration pathways as e.g. generated by highly efficient simple climate models such as MAGICC

and reaching high levels of global warming. Projections account for the inter-impact-model spread of the ISIMIP data set as an indicator of robustness. It may become particularly relevant when impact projections should be included in Integrated Assessment Models (IAM) to estimate their economic effects. Thus, the crop yield emulators were e.g. presented to the IAM community at different workshops (e.g. within the chain of meetings on “Comparing methods and improving the empirical foundations of Agriculture Impacts” at JRC in Sevilla and in Stanford). The “constrained extrapolation approach” for sea level projections has already been applied to estimate the differences in end of the century sea level rise between 2°C and 1.5°C scenarios (Schleussner et al., 2016). To this end, the simple climate model MAGICC was applied to generate a plausible global mean temperature pathway in line with the 1.5°C target. The considered scenario goes beyond the available range of RCP scenarios and demonstrates the demand for simplified methods for extrapolating impacts to emission scenarios not yet covered by complex climate and impact model simulations. Similarly, the “constrained extrapolation approach” for sea level rise will also be applied within the context of the next round of ISIMIP simulations dedicated to provide critical input for the Special Report on the impacts of 1.5°C of global warming (ISIMIP2, Frieler et al., 2016, www.isimip.org). Here it will be used to generate pattern of sea level rise which will be provided as input for impact models describing the risk of coastal flooding. Associated projections will also be provided for the coastal flood projections within HELIX.

4. Acknowledgements

We are grateful to all ISIMIP modelling groups for providing their results and details about the model functioning. We gratefully acknowledge that this project, HELIX, has received funding from the European Union’s Seventh Framework Programme for research, technological development and demonstration under grant agreement no 603864.

5. References

- Church, John A., and Neil J. White. 2011. “Sea-Level Rise from the Late 19th to the Early 21st Century.” *Surveys in Geophysics* 32 (4): 585–602. doi:10.1007/s10712-011-9119-1.
- Dai, Aiguo. 2011. “Drought under Global Warming: A Review.” *Wiley Interdisciplinary Reviews: Climate Change, Advanced Review*, 2 (1): 45–65. doi:10.1002/wcc.81.
- Darwin, Roy, and Darren Kennedy. 2000. “Economic Effects of CO₂ Fertilization of Crops: Transforming Changes in Yield into Changes in Supply.” *Environmental Modeling & Assessment* 5 (3): 157–68. doi:10.1023/A:1019013712133.
- Eyshi Rezaei, E., T. Gaiser, S. Siebert, B. Sultan, and F. Ewert. 2014. “Combined Impacts of Climate and Nutrient Fertilization on Yields of Pearl Millet in Niger.” *European Journal of Agronomy* 55 (April): 77–88. doi:10.1016/j.eja.2014.02.001.

- Frieler, K., R. Betts, E. Burke, P. Ciais, S. Denvil, D. Deryng, K. Ebi, et al. 2016. "Assessing the Impacts of 1.5°C Global Warming – Simulation Protocol of the Inter-Sectoral Impact Model Intercomparison Project (ISIMIP2b)." *Geosci. Model Dev. Discuss.* 2016 (October): 1–59. doi:10.5194/gmd-2016-229.
- Friend, Andrew D., Wolfgang Lucht, Tim T. Rademacher, Rozenn Keribin, Richard Betts, Patricia Cadule, Philippe Ciais, et al. 2014. "Carbon Residence Time Dominates Uncertainty in Terrestrial Vegetation Responses to Future Climate and Atmospheric CO₂." *Proceedings of the National Academy of Sciences* 111 (9): 3280–85. doi:10.1073/pnas.1222477110.
- Gillett, Nathan P., Vivek K. Arora, Kirsten Zickfeld, Shawn J. Marshall, and William J. Merryfield. 2011. "Ongoing Climate Change Following a Complete Cessation of Carbon Dioxide Emissions." *Nature Geosci* 4 (2): 83–87. doi:10.1038/ngeo1047.
- Hay, Carling C., Eric Morrow, Robert E. Kopp, and Jerry X. Mitrovica. 2015. "Probabilistic Reanalysis of Twentieth-Century Sea-Level Rise." *Nature* 517 (7535): 481–84.
- Hempel, S., K. Frieler, L. Warszawski, J. Schewe, and F. Piontek. 2013. "A Trend-Preserving Bias Correction – the ISI-MIP Approach." *Earth Syst. Dynam.* 4 (2): 219–36. doi:10.5194/esd-4-219-2013.
- IPCC. 2013. "Summary for Policymakers, in: Climate Change 2013: The Physical Science Basis, Contribution of Working Group I to the Fifth Assessment Report of the Intergovernmental Panel on Climate Change." In , edited by T.F. Stocker, D. Qin, Gian-Kasper Plattner, M. Tignor, S. Allen, J. Boschung, A. Nauels, Y. Xia, V. Bex, and IPCC AR WGI, 1–100. Cambridge, United Kingdom and New York, NY, USA,: Cambridge University Press.
- Leclercq, P. W., J. Oerlemans, and J. G. Cogley. 2011. "Estimating the Glacier Contribution to Sea-Level Rise for the Period 1800–2005." *Surveys in Geophysics* 32 (4): 519. doi:10.1007/s10712-011-9121-7.
- Lobell, David B., Adam Sibley, and J. Ivan Ortiz-Monasterio. 2012. "Extreme Heat Effects on Wheat Senescence in India." *Nature Clim. Change* 2 (3): 186–89. doi:10.1038/nclimate1356.
- Meehl, Gerald A., Julie M. Arblaster, and C. Tebaldi. 2005. "Understanding Future Patterns of Increased Precipitation Intensity in Climate Model Simulations." *Geophysical Review Letter* 32 (L18719). doi:10.1029/2005GL023680.
- Meinshausen, M., S. C. B. Raper, and T. M. L. Wigley. 2011. "Emulating Coupled Atmosphere-Ocean and Carbon Cycle Models with a Simpler Model, MAGICC6 – Part 1: Model Description and Calibration." *Atmospheric Chemistry and Physics* 11 (4): 1417–1456. doi:10.5194/acp-11-1417-2011.
- Mengel, Matthias, Anders Levermann, Katja Frieler, Alexander Robinson, Ben Marzeion, and Ricarda Winkelmann. 2016. "Future Sea Level Rise Constrained by Observations and Long-Term

- Commitment." *Proceedings of the National Academy of Sciences* 113 (10): 2597–2602. doi:10.1073/pnas.1500515113.
- Müller, Christoph, and Richard D. Robertson. 2014. "Projecting Future Crop Productivity for Global Economic Modeling." *Agricultural Economics* 45 (1): 1574–0862. doi:10.1111/agec.12088.
- Perrette, Mahé, Ricardo Riva, Felix W. Landerer, Katja **Frieler**, Malte Meinshausen. 2013 "A scaling approach to project regional sea level rise and its uncertainties", *Earth Syst. Dynam.*, 4, 11–29.
- Portmann, Felix, T., Stefan Siebert, and Petra Döll. 2010. "MIRCA2000—Global Monthly Irrigated and Rainfed Crop Areas around the Year 2000: A New High-Resolution Data Set for Agricultural and Hydrological Modeling." *Global Biogeochemical Cycles* 24 (GB1011): 24 p. doi:10.1029/2008GB003435.
- Rosenzweig, Cynthia, Joshua Elliott, Delphine Deryng, Alex C. Ruane, Christoph Müller, Almut Arneeth, Kenneth J. Boote, et al. 2014. "Assessing Agricultural Risks of Climate Change in the 21st Century in a Global Gridded Crop Model Intercomparison." *Proceedings of the National Academy of Sciences* 111 (9): 3268–73. doi:10.1073/pnas.1222463110.
- Schlenker, Wolfram, and Michael J. Roberts. 2009. "Nonlinear Temperature Effects Indicate Severe Damages to U.S. Crop Yields under Climate Change." *Proceedings of the National Academy of Sciences* 106 (37): 15594–98. doi:10.1073/pnas.0906865106.
- Solomon, Susan, Gian-Kasper Plattner, Reto Knutti, and Pierre Friedlingstein. 2009. "Irreversible Climate Change due to Carbon Dioxide Emissions." *Proceedings of the National Academy of Sciences* 106 (6): 1704–9. doi:10.1073/pnas.0812721106.
- Warszawski, Lila, Katja Frieler, Veronika Huber, Franziska Piontek, Olivia Serdeczny, and Jacob Schewe. 2014. "The Inter-Sectoral Impact Model Intercomparison Project (ISI-MIP): Project Framework." *Proceedings of the National Academy of Sciences* 111 (9): 3228–32. doi:10.1073/pnas.1312330110.
- Weedon, G. P., S. Gomes, P. Viterbo, W. J. Shuttleworth, E. Blyth, H. Österle, J. C. Adam, N. Bellouin, O. Boucher, and M. Best. 2011. "Creation of the WATCH Forcing Data and Its Use to Assess Global and Regional Reference Crop Evaporation over Land during the Twentieth Century." *Journal of Hydrometeorology* 12 (5): 823–48. doi:10.1175/2011JHM1369.1.
- Wigley, T. M. L. 2005. "The Climate Change Commitment." *Science* 307 (5716): 1766. doi:10.1126/science.1103934.